Single-polymer Brownian motor: A simulation study

Matthew T. Downton,[1] Martin J. Zuckermann,[1] Erin M. Craig,[2] Michael Plischke,[1] and Heiner Linke[2]
[1]*Department of Physics, Simon Fraser University, Burnaby, B.C. V5A 1S6, Canada*
[2]*Materials Science Institute and Physics Department, University of Oregon, Eugene, Oregon 97405, USA*
(Received 14 September 2005; published 18 January 2006)

Numerical simulation is used to study a single polymer chain in a flashing ratchet potential to determine how the mechanism of this Brownian motor system is affected by the presence of internal degrees of freedom. The polymer is modeled by a freely jointed chain with N monomers in which the monomers interact via a repulsive Lennard-Jones potential and neighboring monomers on the chain are connected by finite extensible nonlinear elastic bonds. Each monomer is acted upon by a 1D asymmetric, piecewise linear potential of spatial period L comparable to the radius of gyration of the polymer. This potential is also characterized by a localization time, t_{on}, and by a free diffusion time, t_{off}. We characterize the average motor velocity as a function of L, t_{off}, and N to determine optimal parameter ranges, and we evaluate motor performance in terms of finite dispersion, Peclet number, rectification efficiency, stall force, and transportation of a load against a viscous drag. We find that the polymer motor performs qualitatively better than a single particle in a flashing ratchet: with increasing N, the polymer loses velocity much more slowly than expected in the absence of internal degrees of freedom, and the motor stall force increases linearly with N. To understand these cooperative aspects of motor operation, we analyze relevant Rouse modes. The experimental feasibility is analyzed and the parameters of the model are scaled to those of λ-DNA. Finally, in the context of experimental realization, we present initial modeling results for a 2D flashing ratchet constructed using an electrode array, and find good agreement with the results of 1D simulations although the polymer in the 2D potential sometimes briefly "detaches" from the electrode surface.

DOI: 10.1103/PhysRevE.73.011909 PACS number(s): 87.16.Nn, 05.40.−a, 05.60.Cd, 82.35.Pq

I. INTRODUCTION

Molecular motors are individual molecules or molecular assemblies that convert some form of energy (for example chemical energy) into mechanical work. In living systems, protein motors operating through hydrolysis of nucleotide triphosphates such as ATP [1–4] are instrumental in biological functions including intracellular transport, ion pumping, cell motion, mitosis, protein synthesis, and DNA replication [5,6]. Inspired by biological motors and enabled by nanotechnology, a number of efforts are underway to construct artificial molecular motors. One approach is the use of synthetic chemistry: machine parts that have been synthesized successfully include shuttles consisting of a mobile molecular ring on the axis of a molecule as well as "propellers," "gears," "turn stiles," and "rotors" [7–9]. Alternatively, DNA itself has been used as a versatile building block, and DNA tweezers [10,11] as well as DNA-based linear motors capable of moving along a track [12,13] have been demonstrated.

Molecular motors operate at energies that are comparable to the thermal fluctuations of the surrounding environment. They must therefore function fundamentally differently from macroscopic machines, for which fluctuations are unimportant. From a physics point of view, it is of interest to understand how molecular machines utilize the interplay of nonmechanical energy input, structural changes, and random thermal fluctuations to perform mechanical tasks efficiently and effectively. One approach to answering these questions is to consider systems that explicitly incorporate diffusive steps (thermal fluctuations) as an integral part of the generation of force and motion (Brownian motors [14–19]) and that are simple enough for detailed theoretical and experimental investigation.

One well-studied type of Brownian motor is the "flashing ratchet," in which particles undergoing free diffusion are periodically or randomly subjected to an asymmetric, periodic potential (see Fig. 1). The sequence of free diffusion followed by asymmetric localization leads to a net particle current [20,21]. When used to model a molecular motor, for example, the transporter protein kinesin, the time-dependent, asymmetric potential (the details of which can be made more complex and realistic than those shown in Fig. 1) represents the binding potential along a microtubule. The potential's time dependence reflects the changes in the effective binding potential during the cycle of ATP hydrolysis catalyzed by kinesin [16].

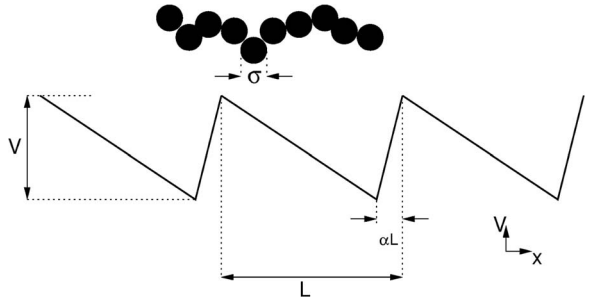

FIG. 1. Schematic diagram of the applied ratchet potential characterized by an asymmetry parameter, α, height, V, and period, L. The potential acts on each monomer of a freely jointed polymer with N monomers, each monomer having approximate dimension, σ.

So far, studies of flashing ratchets in the over-damped limit have focused on the center-of-mass motion of individual point particles (for example, [20–23]), rigid objects made up of two or more coupled particles [1,24] and pairs of harmonically coupled particles [25–27]. These studies demonstrate that the magnitude and direction of current in a flashing ratchet depend critically on the size and shape of the objects being transported.

A topic that has received little attention is the role of the very large numbers of thermally activated internal degrees of freedom that can exist in a molecular motor. Here we extend the flashing ratchet to incorporate explicitly the internal degrees of freedom of a biomolecule into the transport mechanism (see Fig. 1). Specifically, we analyze the case of a polymer in a time-dependent ratchet potential that acts on each of its monomers (for instance, electrostatically) and that has a spatial period, L, which is comparable to the polymer's radius of gyration. Directed polymer motion is then achieved through the interplay of conformational changes imposed on the polymer by the ratchet potential and random, thermally activated conformational changes.

The motivation for this study is twofold. First, we are interested in how the inclusion of internal degrees of freedom into the flashing ratchet will affect the efficiency, velocity, coherence, and force of this system. Addressing these questions is interesting from a fundamental point of view and may also help us to develop an understanding of how the presence of internal degrees of freedom in biological or artificial molecular motors affects their performance in general. Second, we undertake this study with a specific experimental system in mind. We are interested in the feasibility of constructing an artificial single polymer motor based on a large DNA molecule in solution exposed to a time-dependent, spatially periodic, asymmetric, electrostatic potential with a spatial period comparable to the molecule size. If successfully realized, such a system would be capable of carrying a load such as a bead attached to one end of the DNA (similar to a transporter molecule in a living cell) and would allow detailed experimental studies of the performance of an artificial molecular motor. This concept builds on a previous realization of an electrostatic ratchet system for short DNA segments, which was based on the center-of-mass motion of the segments and did not consider the DNA's internal degrees of freedom [28,29].

In this paper, we first describe our numerical model in Sec. II and then discuss its motor performance in Sec. III. Specifically, we identify the model parameters that lead to high motor velocity and analyze the conformational changes that correlate with effective polymer motion. We then characterize the motor velocity, coherence, efficiency, and power both in absolute terms and in comparison to flashing-ratchet motors without internal degrees of freedom. Finally, in Sec. IV A we discuss a specific experimental system that is under construction to realize such a motor and comment on its feasibility.

II. MODEL

A. Model details

The polymer is modeled as a freely jointed chain of monomers using a standard simulation force field consisting of a repulsive Lennard-Jones potential of the form

$$V_{ij}(r_{ij}) = \begin{cases} 4\epsilon\left[\left(\frac{\sigma}{r_{ij}}\right)^{12} - \left(\frac{\sigma}{r_{ij}}\right)^{6}\right] + \epsilon, & r_{ij} \leqslant 2^{1/6}\sigma, \\ 0, & r_{ij} > 2^{1/6}\sigma, \end{cases} \quad (1)$$

acting between all monomers and finite extensible nonlinear elastic (FENE) bonds between neighboring monomers

$$U(r_{ij}) = -\frac{1}{2}k_F R_0^2 \ln\left(1 - \frac{r_{ij}^2}{R_0^2}\right). \quad (2)$$

Here r_{ij} is the monomer-monomer separation. The mass m of each monomer is set to unity and we use σ, ϵ, and $\tau = \sqrt{m\sigma^2/\epsilon}$ to set the length, energy, and time scales. The values k_F and R_0 were chosen to be $30\epsilon/\sigma^2$ and 1.5σ, respectively. This model of a polymer is well studied and has been used previously to model polymer melts [30].

The equations of motion of individual monomers are given by

$$m\ddot{\mathbf{r}}_i = -\gamma\dot{\mathbf{r}}_i + \boldsymbol{\xi}_i(t) - \boldsymbol{\nabla}_i V_p(\mathbf{r}_i) - \boldsymbol{\nabla}_i V_{ext}(t, \mathbf{r}_i), \quad (3)$$

where $\boldsymbol{\xi}_i$ is a random force representing the surrounding solvent and heat bath $[\langle\boldsymbol{\xi}_i\rangle = 0; \langle\boldsymbol{\xi}_i(t)\cdot\boldsymbol{\xi}_j(t')\rangle = 6\gamma kT\delta_{ij}\delta(t-t')]$ with $kT = \epsilon$, γ is the friction coefficient of one monomer, $-\boldsymbol{\nabla}_i V_p = -\Sigma(\boldsymbol{\nabla}_i V_{ij}(r_{ij}) + \boldsymbol{\nabla}_i U(r_{ij}))$ represents the internal polymer forces acting on the monomer as given in Eqs. (1) and (2). The polymer's free diffusion coefficient is given by $D = kT/N\gamma$. $V_{ext}(t, \mathbf{r})$ represents the flashing ratchet potential described below.

Each temporal cycle of the flashing ratchet is set by the localization time, t_{on}, and the free diffusion time, t_{off}, and we use periodic cycling with temporal period $T = (t_{on} + t_{off})$. During t_{off} the ratchet potential is switched off and $V_{ext} = 0$. During t_{on} we use the well-known one-dimensional sawtooth potential shown in Fig. 1. This potential is periodic in the x direction with spatial period L and an asymmetry parameter $0 < \alpha < 1$ defined as in Fig. 1. In addition to the traditional 1D ratchet potential described above, towards the end of the paper we will use a more realistic 2D potential in order to explore the experimental feasibility of our single polymer motor concept (Sec. IV B).

B. Scaling to experiment

A key motivation for the study of the polymer motor developed here is to provide information about suitable parameters and about the expected performance of the planned experimental realization of such a motor. In order to translate the model's scaled, dimensionless quantities into absolute numbers, we consider an experiment that will use a periodic array of electrodes to generate an electrostatic ratchet potential that can be switched on and off [28,29] (for more details, see Sec. IV B). For the polymer, we consider lambda-phage DNA (λ-DNA), which in aqueous solution has a net negative charge, forming a polyelectrolyte, such that it can be manipulated by an electrostatic potential.

Our approach is to relate the physical properties of the persistence length of double-stranded (ds) DNA to those of a persistence length of the model polymer in the simulation.

TABLE I. Scaling relationships between the Brownian dynamics simulation model and double stranded DNA.

Parameter	BD model	dsDNA (l_p=50 nm)	dsDNA (l_p=90 nm)
Length	$\sigma=1$	$\sigma=50$ nm	$\sigma=90$ nm
Energy	$\epsilon=kT=1$	$\epsilon=kT=25.9$ meV=4.14 pN nm	$\epsilon=kT=25.9$ meV=4.14 pN nm
Force	ϵ/σ	$kT/\sigma=0.083$ pN	$kT/\sigma=0.046$ pN
Charge	$q=1$	$q=-17e$	$q=-30e$
Potential	$\epsilon/q=1$	$kT/q=1.5$ mV	$kT/q=0.86$ mV
Diffusion coefficient	$D=kT/\gamma=1$	$D=3.3\times10^{-11}$ m^2 s^{-1}	$D=2.2\times10^{-11}$ m^2 s^{-1}
Drag coefficient	$\gamma=1$	$\gamma=kT/D=1.3\times10^{-10}$ kg s^{-1}	$\gamma=kT/D=1.9\times10^{-10}$ kg s^{-1}
Time	$\tau=\sigma^2/D=1$	$\tau=\sigma^2/D=7.6\times10^{-5}$ s	$\tau=\sigma^2/D=3.7\times10^{-4}$ s

Baumann *et al.* [31] used stretching experiments and worm-like polymer chain (WLC) models to determine that λ-DNA (48.5 kbp) has a persistence length $l_p\approx90\pm10$ nm under relatively low-salt conditions (1.8 mM NaCl), while the persistence length is shorter for higher ionic strength. This value was found for both weakly and strongly extended DNA, in agreement with other findings that the persistence length of λ-DNA is independent of stretching force [32]. The model used in our simulations is based on a Rouse-like polymer chain with excluded volume interactions equivalent to a self-avoiding walk. Slater *et al.* [33] point out that such chains become Gaussian chains in the strong stretching limit with a persistence length equal to the bond length, $b=0.97\sigma$. In addition, we find in Brownian dynamics simulations that the bond angle correlation function $\langle\mathbf{t}_i\cdot\mathbf{t}_j\rangle$ for our Rouse-like polymer decays by a factor of $1/e$ as a function of displacement within about one σ, again suggesting that $l_p\sim\sigma$ in our model. A reasonable estimate for the scaling relationship for λ-DNA is therefore $l_p\approx\sigma$ where $l_p\approx90$ nm. Note, however, that the established value for the persistence length under low-salt conditions for much shorter segments of dsDNA (less than 1 kbp≈300 nm) is approximately 50 nm. In the following, we will therefore use $\sigma=90$ nm and $\sigma=50$ nm as the upper and lower bounds of our unit of length and establish separate scaling relationships for energy, force, and time based on each of these two values.

The model unit of energy is $\epsilon=kT=1$, and the unit of force is kT/σ. Units of electric potential and electric field can be defined as kT/q and $kT/q\sigma$, respectively, where each monomer interacts with the applied ratchet potential through a charge $q=1$. The charge per base pair of dsDNA is quoted as $-0.1e$ [34] under normal salt conditions, with 0.3 nm per base pair. Consequently we take the linear charge density as $-17e/\sigma$ and $-30e/\sigma$, corresponding to $l_p=50$ nm and $l_p=90$ nm, respectively. Using $kT=25.9$ meV=4.14 pNnm at room temperature, the resulting units for force, potential, and electric field based on the two values for the persistence length are summarized in Table I.

The model time unit is set by $\tau=\sqrt{m\sigma^2/\epsilon}$. However, in order to match the unit time to experiment we prefer a relationship based on measurable quantities that are independent of mass. We choose to write the unit time as $\tau=\sigma^2/D$ where D is the translational diffusion constant of a monomer of unit length σ. Using the Einstein relation $D\gamma=kT$ and $\epsilon=kT=1$, it can be shown that the above two definitions of τ are equivalent to a third, namely the momentum relaxation time $\tau=m/\gamma$.

We can match the unit time, $\tau=\sigma^2/D$, to experiment using $\sigma=l_p$ as found above, and $D=D_p$, where D_p is the linear diffusion constant of a segment of dsDNA of length l_p. A table of experimental values of the linear diffusion constant of dsDNA was compiled by Liu and Giddings [35] for a wide range of dsDNA segment sizes. By interpolating between data points in the appropriate size range, we estimate $D_p\approx3.3\times10^{-11}$ m^2/s for $l_p=50$ nm and $D_p\approx2.2\times10^{-11}$ m^2/s for $l_p=90$ nm. Based on these values, the unit of time is $\tau=\sigma^2/D\approx7.6\times10^{-5}$ s and $\tau\approx3.7\times10^{-4}$ s, for $l_p=50$ and 90 nm, respectively (see Table I).

III. RESULTS

A. General characteristics

Before beginning our characterization of the polymer motor, we justify our choice of parameters. The potential strength, V, in a flashing ratchet should be at least several kT in order to localize particles successfully during t_{on} and, unless specified otherwise, we will use $V=4kT=4\epsilon$ throughout this paper. As we will show below, the motor velocity increases for larger choices of V, but $V\gg kT$ is not realistic for most experimental systems of interest. For the asymmetry parameter α of the ratchet potential, we choose $\alpha=0.1$ throughout the paper (see Fig. 1). The overall contour length of the polymer used is determined by the total number of monomers, N, and as an initial value we use $N=50$. The spatial ratchet period, L, should be larger than a monomer length, σ, and we are most interested in values of L comparable to the polymer's radius of gyration, which we find to be $R_g=4.7\sigma$ for $N=50$.

The next step in characterizing the polymer motor is to establish suitable switching times, t_{on} and t_{off}, for the "flashing" of the ratchet potential, which we choose to do periodically. Beginning with t_{on}, we wish to expose the polymer to a ratchet potential for a time that is sufficient to localize fully a polymer that is initially in a random configuration (note that this is not necessarily the optimal choice for maximum motor velocity). In Fig. 2, we show the velocity of the polymer center of mass, averaged over many time cycles, as a

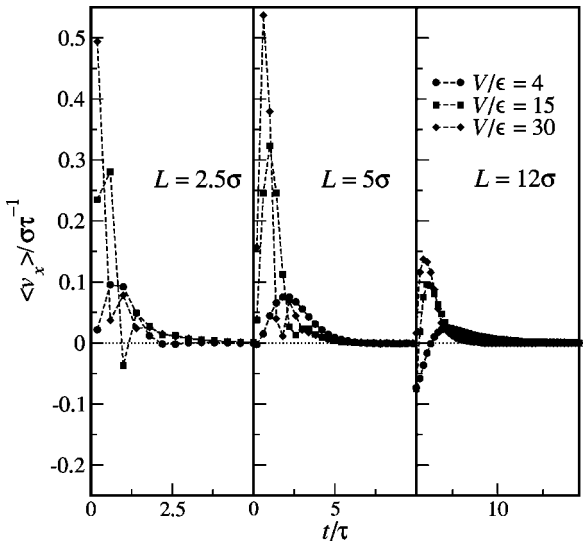

FIG. 2. Velocity of the polymer center of mass as a function of time after the ratchet potential is switched on, averaged over repeated cycles of the potential (N=50; from left to right: L=2.5σ,5.5σ,12σ).

function of time t after the ratchet potential is switched on for three values of the spatial period, L, and for three different barrier heights. Increasing the strength of the localizing potential, V, generally decreases the time needed to confine the polymer, while confinement slows with increasing L at fixed V, because the localizing force becomes smaller. It can also be seen that the relaxation processes have finished for all L and V by $t_{on}=20\tau$. This value is chosen throughout the rest of this study.

In order to make a good choice for the free diffusion time, t_{off}, we show in Fig. 3 the time-averaged polymer velocity (N=50) as a function of ratchet period, L, for a range of different choices of t_{off}. Within the parameter range investigated, we observe the highest velocities for $t_{off} \approx 20 \pm 10\tau$, and, unless specified otherwise, we will use $t_{off}=20\tau$ throughout this paper.

To obtain a general idea about the influence of the potential strength, we show in Fig. 4 the time-averaged polymer

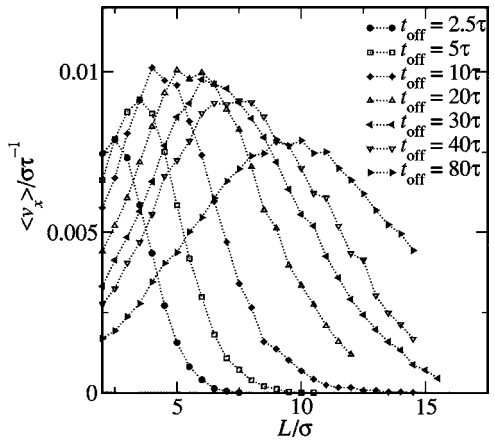

FIG. 3. Polymer center-of-mass velocity averaged over many cycles as a function of L for t_{off}=2.5τ, 5τ, 10τ, 20τ, 30τ, 40τ, 80τ (t_{on}=20τ; N=50).

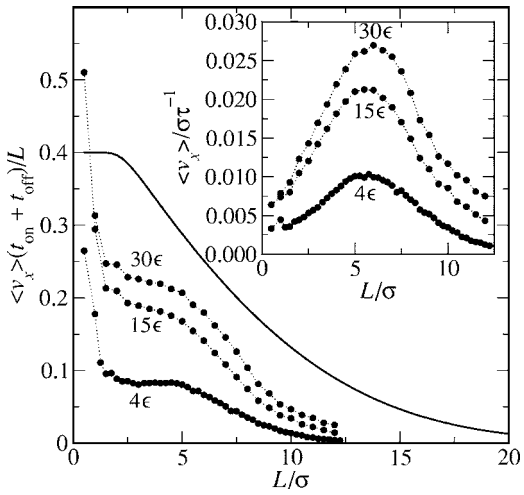

FIG. 4. Average velocity of polymers of contour length, 50σ, and total drag coefficient, γ=50, for different values of V against L in units of ratchet periods per time cycle (main figure) and in absolute units (inset). $t_{on}=t_{off}=20\tau$. Thick solid line: analytical calculations for a single particle with drag coefficient γ=50 assuming perfect confinement during t_{on}.

velocity for several different values of V, as a function of L. The inset shows the absolute velocities in units of (σ/τ), while the main figure shows the velocities in units of $L/(t_{on}+t_{off})$ which gives the number of ratchet periods the polymer moves per time cycle. We find that the average velocity increases with stronger confinement as expected from a single particle picture because, for weak confinement, the particle distribution will be skewed towards the shallow side of the potential. This reduces the effective potential asymmetry and lowers the particle current. Increasing the height of the potential barrier increases the effective asymmetry towards the actual value, α. In the case of a polymer straddling several periods, there is the additional effect that short segments of the polymer (such as the trailing end of a polymer) can be pulled over the potential barrier by larger segments in the adjacent potential well. To put the absolute velocities into context, we show in Fig. 4 the velocity expected for a single particle with drag coefficient 50γ (the same as the overall drag coefficient of the polymer), calculated analytically assuming perfect confinement ($V \gg kT$) during t_{on} as described by Ajdari and Prost [20]. We note that in the ideal case (α=0, $L^2 \ll 2Dt_{off}$, where D is the single particle diffusion constant, and $V \to \infty$) a flashing ratchet displaces a particle on average by 0.5L during each cycle. As one would expect, the partially confined polymer is slower than the perfectly confined single particle across the entire range, except in the limit of very small L. In this range, however, the polymer simulations are at the edge of reasonable physical limits, because the ratchet period becomes comparable to the monomer length, and a more realistic polymer model, such as the wormlike chain, is required for conclusive results. A more detailed comparison of polymers and single particles will be presented below (Sec. III C).

B. Mode of operation

The dependence of polymer velocity on the number, N, of monomers is shown in Fig. 5. Strikingly, over more than an

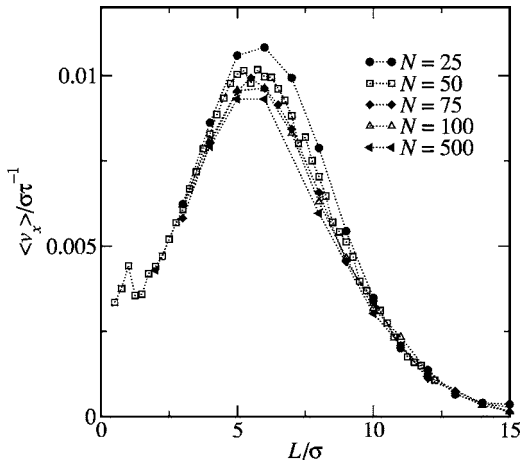

FIG. 5. Average velocity of the polymer for $t_{on}=t_{off}=20\tau$ for values of N varying by more than one order of magnitude. Although the velocity decreases slightly with increasing N, the position of the peak remains at approximately $L=5\sigma$.

order of magnitude variation in polymer contour length and its center-of-mass diffusion coefficient, there is very little variation in polymer velocity. In fact, all polymers exhibit almost the same dependence on spatial ratchet period, L, with a velocity peak at $L\approx 5\sigma$. This consistent behavior and the independence of velocity from the number, N, of monomers indicate that the mode of transport is not the same as in the traditional flashing ratchet (which relies on center-of-mass diffusion) but rather that the polymer's internal degrees of freedom are important [49].

In order to analyze the changes in internal polymer configuration that are involved in polymer motion, we expand the polymer conformation in Rouse modes [36] which, for a polymer of N monomers with center of mass $\mathbf{r}_{cm}$, have the following form:

$$\mathbf{X}_p = \frac{1}{N}\sum_{i=1}^{N} \cos\left(\frac{p\pi(i-1)}{N-1}\right)(\mathbf{r}_i - \mathbf{r}_{cm}). \tag{4}$$

For an isolated ideal polymer in solution, each of these normal modes, $\mathbf{X}_p$, executes an independent random walk. Excluded volume effects will lead to correlations between modes, although these can be expected to be small for long wavelengths. Here we will consider the x components of the lowest amplitudes, X_{x1} and X_{x2}, which give information on the projection of shape and orientation of the polymer onto the x axis. Specifically, X_{x1} represents extension of the ends of the polymer away from its center of mass, and X_{x2} is large for configurations which have a single loop around the center of mass.

We first apply the Rouse mode analysis to the case of a relatively large spatial ratchet period, namely $L=12\sigma$, which is to the right of the velocity peak in Fig. 5. In Fig. 6(a), we show an example for a displacement trace over 2000 time cycles, each of 40τ duration. Overall, progress is rather slow (the polymer takes a total of only six well-defined steps of length $L=12\sigma$) and between steps the polymer center-of-mass is well localized at the potential minima. In Figs. 6(b) and 6(c), we show the corresponding time traces of the polymer's Rouse modes, X_{x1} and X_{x2}, respectively. Note that there is a very clear correlation between stepping events in Fig. 6(a) and high amplitudes in the x components of the lowest Rouse modes. Closer analysis of stepping events, which gradually take place over several time cycles, indicates that translation is characterized by long-lasting conformations in which the polymer extends across two ratchet periods (as indicated by the marked increase in X_{x1}). Between stepping events, the polymer is localized, without extension in the x direction (an illustrative animation is available [50]).

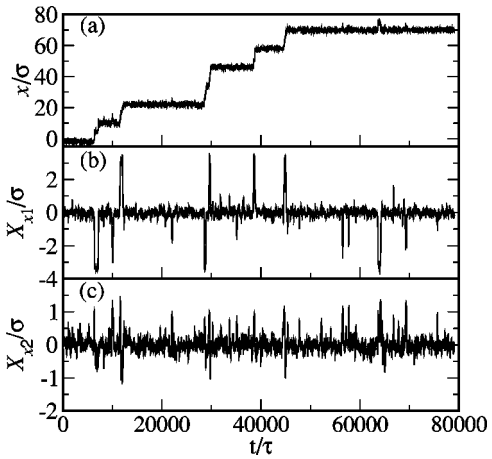

FIG. 6. (a)–(c) Trace of the polymer position with time along with corresponding information on the polymer conformation ($L=12\sigma$; $t_{on}=t_{off}=20\tau$).

As shown previously in Fig. 5, we observe the highest average polymer velocities for all N at $L=5\sigma$ and in Fig. 7 we show an analysis of the mode of operation in this case. Compared to the case of long ratchet periods, the polymer's translational progress is much faster, and the stepping behavior is much less pronounced as a close examination of the data reveals that there are no resolved steps. In addition, we almost continuously observe high amplitudes of the two lowest Rouse modes, indicating that the polymer tends to be

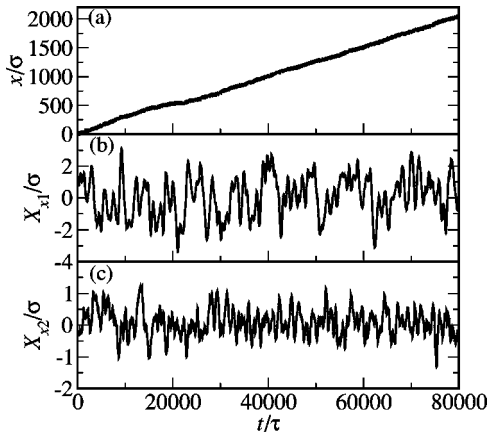

FIG. 7. (a) Trace of the polymer position with time and the corresponding values of the first and second Rouse modes [(b) and (c)] ($L=5\sigma$; $t_{on}=t_{off}=20\tau$).

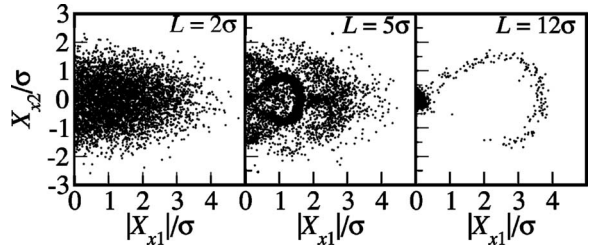

FIG. 8. Second Rouse mode versus absolute value of the first Rouse mode at the end of the localization period of the external ratchet potential for different values of L.

stretched out most of the time and only rarely collapses into individual wells.

In Fig. 8, we compare the correlation of Rouse modes X_{x1} and X_{x2} at the end of the localization periods. In both of the cases considered so far ($L=5\sigma$ and $L=12\sigma$), some correlations between the two Rouse modes are visible, indicating that the presence of the ratchet has a strong influence on the polymer conformation. In the case $L=12\sigma$, most polymers have amplitude zero in both lowest Rouse modes at the end of t_{on}, indicating that the polymer is collapsed into one well. During stepping events, however, half-stretched loops exhibit an asymmetry with respect to $X_{x2}=0$; projected onto the x axis, polymer loops form in the forward direction but not backwards into the previous well. The rich correlations for $L=5\sigma$ show that the polymer spends a lot of time stretched out over several periods, facilitating transport, with specific configurations appearing frequently. In the case of the smallest ratchet period ($L=2\sigma$), we find that transport is basically a noisy, biased random walk with frequent back-stepping. No specific conformations appear.

C. Polymer motor versus single-particle ratchet

Brownian motors in general require diffusion of the motor as part of the operating principle. Because the diffusion constant decreases with motor size, there are limits on the size of single-particle Brownian motors that can operate effectively. One important motivation for the study of a polymer ratchet is the notion that the characteristic time for thermally activated reconfiguration of the polymer's internal degrees of freedom does not necessarily change with the overall size of the polymer. In other words, a Brownian motor that makes use of internal degrees of freedom may be sustainable for large polymers.

In Fig. 9, we quantitatively compare the velocities of a polymer of contour length, $N\sigma$, and with total drag coefficient, $N\gamma$, to point particles with the same drag coefficient as a function of N. As expected, for all L the velocity of the point particle decays quickly with increasing N, as the point particle loses its ability to diffuse during t_{off}. In contrast, the polymer is found to maintain its ability to move. Interestingly, even in the case of small N, where both the polymer and the single particle make use of center-of-mass diffusion, internal degrees of freedom and finite size are an advantage. In the case $L=12\sigma$, the polymer velocity peaks for $N=3$ at a velocity twice that of a point particle with the same drag coefficient.

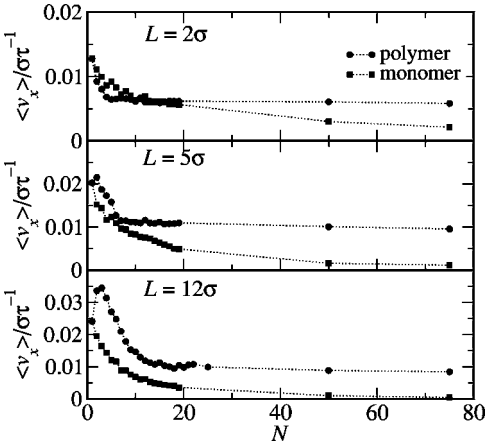

FIG. 9. Average velocity of polymers with drag coefficient, $N\gamma$, as a function of N for different ratchet periods, compared to a point particle with the same drag coefficient ($t_{\mathrm{on}}=t_{\mathrm{off}}=20\tau$, $V=4\epsilon$).

D. Performance

In this section we discuss the polymer motor's performance characteristics in terms of coherence, stall force, motor power, and efficiency.

1. Coherence

As shown previously in Fig. 3, the average motor velocity, $\langle v_x\rangle$, is determined by the choice of t_{off}, which sets the time during which free diffusion takes place. The central role of diffusion, and the related absence of tight coupling between ratchet cycling and stepping events, lead to a finite dispersion

$$D_{\mathrm{eff}}=[\langle x^2(t)\rangle-\langle x(t)\rangle^2]/2t, \tag{5}$$

characteristic of Brownian motors [16,18,37]. In order to quantify the dispersion (diffusion) relative to the ensemble-averaged drift, a dimensionless quantity called the Peclet number [38] may be calculated, which represents the "coherence" of motor transport. The Peclet number is

$$\mathrm{Pe}\equiv\frac{|\langle v_x\rangle|l}{D_{\mathrm{eff}}}, \tag{6}$$

where l is a relevant length scale chosen to determine if dispersion or motor action dominate for transport over this distance and $\langle v_x\rangle$ is the average velocity in the x direction.

We now use these tools to examine the polymer motor's ability to perform transport reliably. We previously noted (see Fig. 3) that the average velocity, $\langle v_x\rangle$, as a function of L peaks for larger values of L as t_{off} is increased, and that the peak velocity is highest around $t_{\mathrm{off}}\approx 20\tau$. For comparison, we show in Fig. 10(a) the dispersion D_{eff} for $N=50$. For small t_{off}, D_{eff} peaks as a function of L at roughly the same value of L as $\langle v_x\rangle$ (see Fig. 3) and, as one might expect, D_{eff} increases with t_{off} (see Fig. 10). Interestingly, for $t_{\mathrm{off}}<20\tau$, D_{eff} is smaller than the polymer's free diffusion constant, $D=0.02\sigma^2/\tau$, as there is only a little time for diffusion between localization periods. For high t_{off}, however, the dispersion is enhanced to values much higher than the bulk values

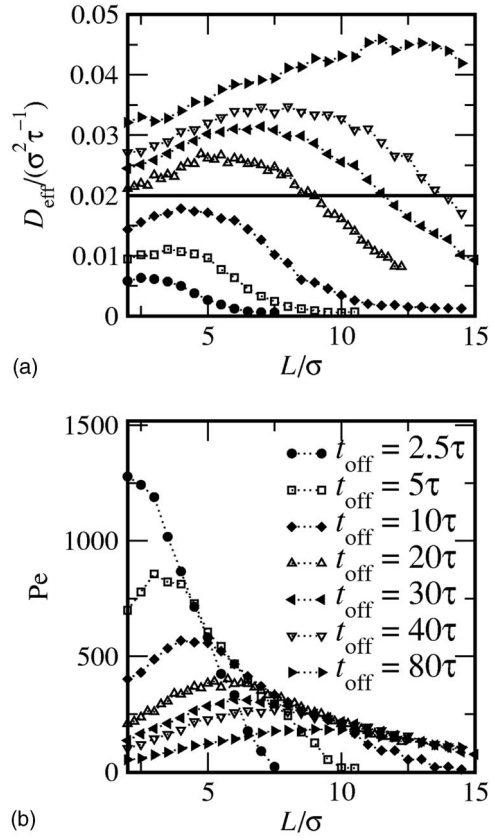

FIG. 10. Dispersion and Peclet number for $t_{\rm off}=2.5$, 5, 10, 20, 30, 40, and 80τ for $N=50$ and $t_{\rm on}=20\tau$. (a) Dispersion, $D_{\rm eff}$, as a function of L. The diffusion constant $D=0.02\sigma^2/\tau$ of a free polymer is indicated as a horizontal line. (b) Pe, calculated for transport over a distance $l=1000\sigma$.

as the diffusion is amplified by the action of the ratchet.

To determine the relative strengths of motor velocity and motor dispersion, we calculate Pe according to Eq. (6) using $l=1000\sigma$ [Fig. 10(b)]. Devices of this length could conceivably be fabricated. Based on the scaling scheme for dsDNA given in Sec. II B and Table I, the length, l, corresponds to translation by the motor of 50–100 μm. The chosen value of l is independent of L, allowing different devices to be compared and it depends on the only well-defined length scale, σ, in the polymer motor. Due to the relatively weak dependence of $D_{\rm eff}$ on L [Fig. 10(a)], the Peclet number peaks for each $t_{\rm off}$ roughly at the same L as $\langle v_x\rangle$ (Fig. 3). However, the strong dependence of $D_{\rm eff}$ on $t_{\rm off}$ means that a substantial improvement of Pe can be attained at a relatively small cost in terms of reduction in motor velocity when small values of $t_{\rm off}$ are chosen.

Note that a similar trade-off exists between the Peclet number and the motor efficiency, η(see Sec. III D 3); η is higher for $t_{\rm off}=20\tau$, where Pe is relatively small, than for $t_{\rm off}=10\tau$, where Pe is relatively large, indicating that the energy cost of reliable transport is high. For details, see Fig. 13(a) and Sec. III D 3.

2. Load force

We now characterize the single-polymer motor in terms of the most important task of a motor in the strictest sense, its ability to perform work on an external agent, and examine two ways of performing work. First, in the present section, we consider motion against an external force, F, that acts on the motor itself, that is, work output in the thermodynamic sense. Second, in Sec. III D 4, we study the motor's ability to move an object (such as a bead with finite drag coefficient) through a viscous medium, similar to the work performed by a tug boat or by a biological transporter protein.

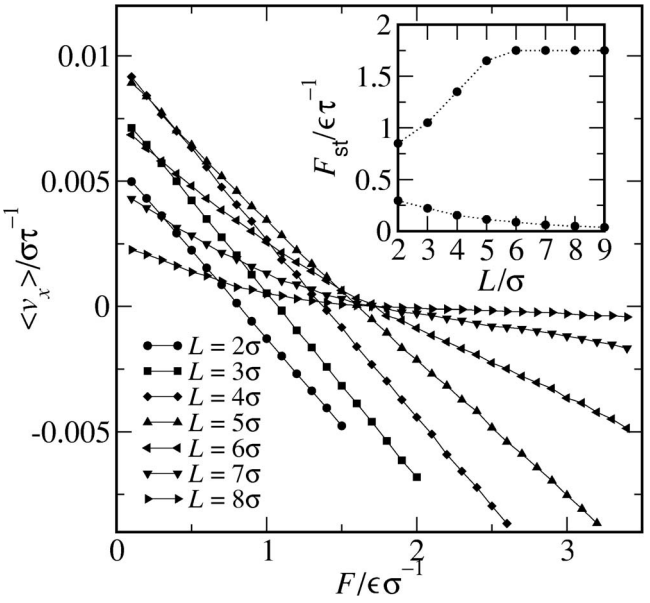

FIG. 11. Force-velocity response curves for a flashing ratchet motor in an external field for different ratchet lengths ($t_{\rm on}=20\tau$; $t_{\rm off}=10\tau$; $N=50$). Inset: Stall force of the polymer as a function of L (circles) and single particle with drag coefficient, 50γ (squares).

To evaluate the motor's ability to do work against an external load force, we apply a force of magnitude F/N to each monomer in the negative x direction and determine $\langle v_x\rangle$ as a function of the total applied force F. The resulting force-velocity curve is shown in Fig. 11 for different values of L. As expected, increasing F reduces $\langle v_x\rangle$ until the polymer stalls at a critical value, $F_{\rm st}$. For low values of L, the response to the external field is linear, indicating that the motor's capability to push forward does not depend on velocity. In this regime, the force-response curves for different values of L are parallel, that is, the mobility does not depend on L.

With increasing L the response becomes nonlinear for forces close to $F_{\rm st}$ and the force-velocity curve is asymmetric around the $\langle v_x\rangle=0$ axis. In the data given in Fig. 11, there is a large region where the velocity is negative and the mobility of the molecule in response to the external field is substantially smaller than elsewhere.

The inset to Fig. 11 shows the polymer's stall force as a function of L, as well as that of a single particle with the same drag coefficient, 50γ, in the same flashing ratchet potential. For the single particle, one expects a stall force of order $F_{\rm st}=kT/\alpha L$, because diffusion over the distance αL becomes unlikely if work of more than kT must be performed. Consequently, one expects the stall force to decrease roughly as $1/L$, as observed. In contrast, the stall force for the polymer *increases* for small L up to about $L=5\sigma$, in line

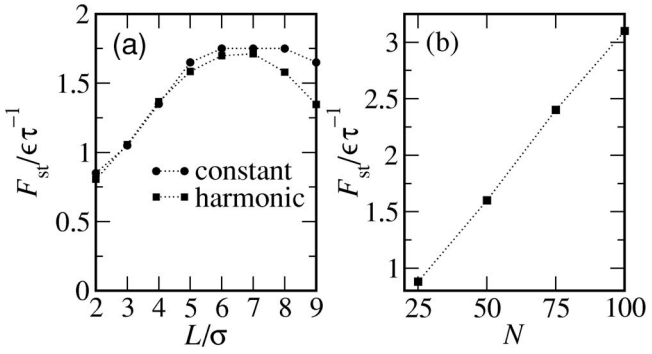

FIG. 12. (a) Comparison of the stall forces calculated from load velocity curves using a constant force (dots) and using a harmonic potential (squares). For the harmonic potential method the value is found by averaging over ten independent simulations of polymers translating against a spring with constant $\kappa=0.01\epsilon/\sigma^2$. (b) Stall force as a function of N calculated using the harmonic-potential method ($t_{on}=20\tau$; $t_{off}=10\tau$; $L=5\sigma$).

with the increase of the motor's zero-force velocity for these values of L (see Fig. 5). For L in the range 5σ to 10σ the stall force levels out about one order of magnitude higher than the stall force for point particles at the same value of L. This may be understood by remembering that in this range of L the diffusion of *part of the polymer* against the external force over the distance αL is sufficient to induce a stepping event (see Sec. III B). One therefore expects the stall force for a polymer in this range to exceed the single-particle stall force, as observed. In the limit of large L, the polymer should increasingly behave like a single particle, and we expect the stall force to decrease as $1/L$ [51].

An alternative method for calculating the force-velocity response of the polymer is to apply to each monomer a spatially dependent force of the type $f=-\kappa x_{cm}$, where x_{cm} is the center of mass, such that the total force on the polymer is of magnitude $F=N\kappa x_{cm}$. This method has been used both theoretically [39,40] and experimentally [41]. The key advantage from a simulation perspective is that it is not necessary to estimate the value of F_{st} prior to the simulation run; the polymer will translate in the x direction until the average "force" generated by the ratchet balances the external field. This is computationally significantly faster than scanning through each value of F in turn. In Fig. 12(a) we compare the stall forces calculated by the two methods. The harmonic method agrees well with the stall forces obtained from the load-velocity curves for shorter ratchet lengths, but tends to underestimate f_{st} with increasing L. In this limit, the dynamics in the harmonic potential slow down considerably, with the polymer taking increasingly longer times to reach a position where the opposing forces are balanced, making estimation of the stall force difficult.

A study of the stall force of a polymer motor as a function of N calculated using the harmonic-potential method is shown in Fig. 12(b). The stall force increases linearly as a function of N, that is, a longer polymer can move against larger forces. This is again in contrast to the behavior of single particles in a flashing ratchet which lose their ability to diffuse with increasing size.

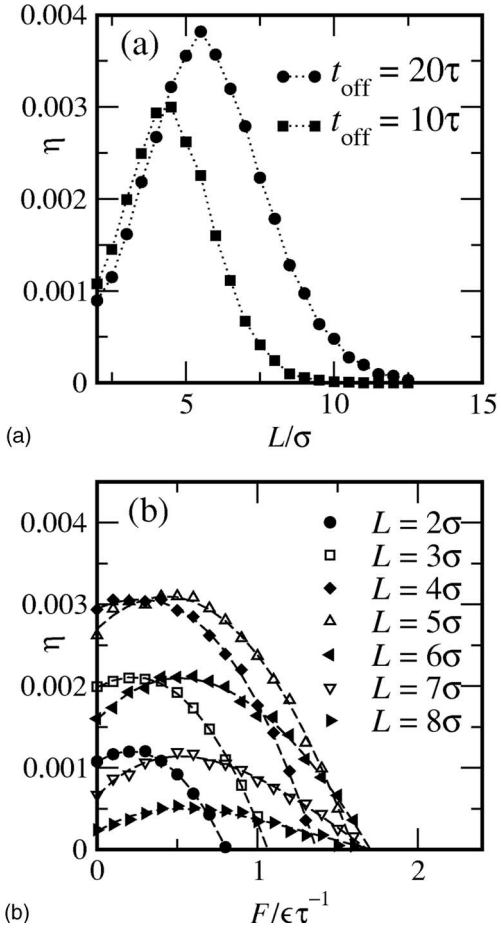

FIG. 13. (a) Rectification efficiency calculated using Eq. (7) for zero external force. (b) Efficiency as a function of force ($N=50$; $t_{on}=20\tau$).

3. Efficiency

Of key interest to the performance of molecular motors is the efficiency with which they perform work. A number of definitions for the efficiency of Brownian motors have been put forward [37,42–46]. Here we use the "rectification" efficiency [45] of a Brownian motor, defined as the ratio [43,45]

$$\eta=\frac{F\langle v_x\rangle+\gamma\langle v_x\rangle^2}{\langle\Delta E\rangle/(t_{off}+t_{on})}, \tag{7}$$

where ΔE is the absolute value of the change in the polymer's (ratchet) potential energy during t_{on} such that the denominator of Eq. (7) is the power input. The numerator has been proposed by Derényi, Bier, and Astumian [43] based on the minimum power required for a motor with total drag coefficient γ to move at average velocity $\langle v\rangle$ against a load force F, and has been derived by Suzuki and Munakata [45] by considering an energy balance for separate terms of the Langevin equation.

In Fig. 13(a), we show the rectification efficiency for the case of zero load force [$F=0$ in Eq. (7)] as a function of L. As expected, the efficiency peaks at the same value of L as the velocity (see Fig. 3). Interestingly, the maximum efficiency for $t_{off}=20\tau$ is higher than for $t_{off}=10\tau$, even though

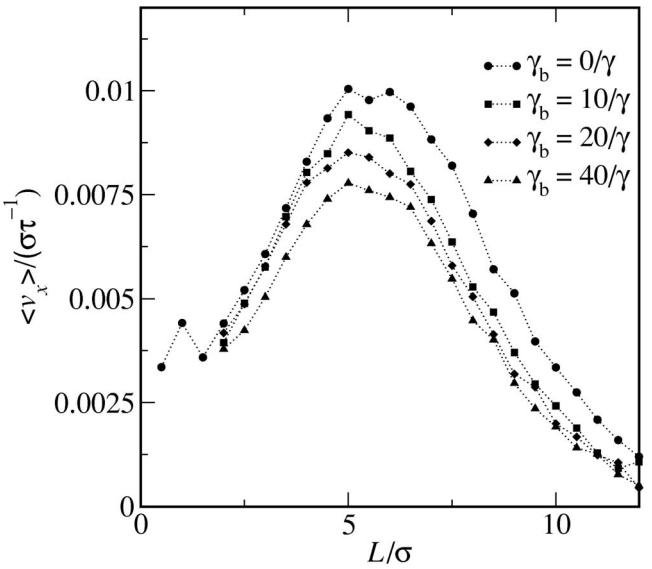

FIG. 14. Average velocity of the polymer for different drag coefficients, γ_b, of a bead attached to one end of the polymer ($t_{on}=t_{off}=20\tau$; $N=50$).

the maximum velocity is similar for the two cases. This difference can be interpreted as follows: if roughly equal work is performed by the ratchet on the polymer in both cases to localize the polymer, this is a higher proportion of the total ratchet cycle for the shorter t_{off}. Overall, the rectification efficiency is small (fractions of a percent) compared to single particles in a flashing ratchet, where η is approximately 5%–10% [44,45,47], indicating that extra work is being performed by the ratchet potential on the polymer internal degrees of freedom, leading to a reduction in efficiency [37].

In Fig. 13(b), the rectification efficiency is shown as a function of a finite load force F/N applied to each monomer. Overall, the efficiency decreases as a function of L for $L>5\sigma$, as is expected since the velocity decreases as a function of L in this range. For small L, where the load-velocity curves shown in Fig. 11 are linear, the rectification efficiency is approximately parabolic as a function of the force, peaking typically for $F\sim 0.5$ and falling continuously to zero at the stall force. For larger L, where the velocity response in Fig. 11(a) is not linear, the efficiency falls off more slowly than quadratically with increasing F.

4. Transporting a load against viscous drag

One task of an experimental artificial molecular motor might be to transport a cargo along a track. The model described in Sec. II can be modified in a simple way by adding a drag bead at one end that is passive to the ratchet potential. Hydrodynamic considerations are important in this situation, especially if the attached bead is much larger than the polymer's persistence length, but are neglected at present.

The polymer velocity versus ratchet length for polymers attached to beads of three different drag coefficients, γ_b, is given in Fig. 14. Simulations were also performed with beads which were much larger than the diameter of the polymer monomers, but no significant changes of $\langle v \rangle$ due to the excluded volume were observed. Overall, the dynamics of the polymer is relatively unaffected by the addition of a load to transport and it is worth noting that, although adding a bead with friction coefficient $\gamma_b=40\gamma$ decreases the diffusion coefficient of the polymer by a factor of 1.8, the overall velocity decreases by only 1.25, showing that the polymer is able to transport a load effectively.

IV. EXPERIMENTAL FEASIBILITY

In this section, we discuss the feasibility and expected performance of an experimental realization of a single-polymer motor. We consider an electrostatic ratchet potential created by a two-dimensional array of asymmetrically spaced, interdigitated electrodes on a substrate such as silicon. This system was used previously by Bader and coworkers [28,29,48], who suspended short pieces (10 to 50 base pairs long) of single-stranded (ss) fluorescently marked DNA in water. The solution containing the electrically charged ssDNA was confined to a micro-chamber on top of the electrode array, which was used to create a time-dependent, asymmetric electrostatic potential. Net transport was observed using fluorescence microscopy. In this experiment, the ratchet period was of the order of $L\sim 10$ μm, which is several orders of magnitude larger than the ssDNA contour length ($\sim$10 nm).

In contrast, we examine the case of a polymer ratchet where the contour length, $N\sigma$, exceeds L and where $L\approx R_g$, as considered in the model above. We quantitatively discuss the expected performance of a dsDNA-based single polymer motor (Sec. IV A) and confirm whether key results obtained using our 1D model potential are valid also for a more realistic 2D electrostatic potential.

A. Quantitative discussion

Our numerical studies indicate that the velocity of a polymer motor reaches a maximum at $L\approx 5-7\sigma$ for $t_{on}=t_{off}=20-40\tau$ (see Fig. 3). The maximum velocity is predicted to depend little on N (Fig. 9), and we consider using $N\approx 100$, corresponding to a 9 μm long section of λ-DNA (approximately 30 kbp) with a persistence length of 90 nm (see Sec. II B and Table I). A ratchet potential with $L\approx 5-7\sigma$ then corresponds to a ratchet period (pitch) of $L\approx 500-600$ nm and a center-to-center distance between the closest spaced electrodes of $\alpha L=0.1L\sim 50-60$ nm. These dimensions can realistically be achieved by electron-beam lithography. Based on the dynamics of the model polymer, a suitable cycle time for the ratchet potential is $(t_{on}+t_{off})\approx 40-80\tau \approx 15-30$ ms, corresponding to a cycling frequency of 30–60 Hz. The potential strength used in the model ($V=4kT$) corresponds to an effective electrode potential of about $4kT/q\approx 3$ mV, and to electric fields of order 3 mV/50 nm=0.6 V/μm.

The estimated velocity under these conditions is about 0.01 σ/τ (Fig. 9), corresponding to 2 μm/s, comparable to the velocity of biological linear motors such as myosins or kinesins [4]. For the polymer motor, this velocity corresponds to about three ratchet periods per second and, given a radius of gyration of order $R_g\approx 1$ μm, the polymer would

translocate by a distance comparable to its own size about every second. Motion of this order of magnitude should be observable by fluorescence microscopy.

The polymer motor's stall force is predicted to be approximately 2 kT/σ (Fig. 11) or about 0.1 pN, an order of magnitude smaller than that observed for linear, biological motors (1.5 pN for myosin II, 3 pN for conventional kinesin [4]). Note, however, that the stall force for the polymer motor can be increased by increasing N and it scales with $1/\sigma$, indicating that a polymer with a shorter persistence length (and using a ratchet potential with correspondingly shorter L) would have a proportionally larger stall force. In this context, it is interesting to note that the work done by the polymer per step (per ratchet period, L) close to stall conditions is about $LF_{st} \approx 5\sigma(2kT/\sigma) = 10kT$, similar to biological motors that have a typical step size of several nanometers and that also do work of the order of several kT per step [4], albeit with much higher efficiency (on the order of 20%–30%) compared to the polymer motor.

Figure 14 further predicts that a polymer motor is capable of transporting a bead or vesicle with a drag coefficient of about 20γ, corresponding to a bead of 0.4 μm diameter, with almost unreduced velocity. This prediction can be tested by using, for example, biotin-strepdavidin binding to attach a correspondingly functionalized polystyrene bead to one end of the DNA.

In conclusion, based on our model, we predict that a polymer motor as described above can conceivably be experimentally realized and observed. Note, however, that our model does not include hydrodynamic interactions, which are likely to slow the polymer dynamics, presumably reducing the predicted velocity of the polymer as well as the stall force. On the other hand, the choice of t_{on} in the present model was based on complete polymer localization, and a shorter t_{on} might be a better choice for maximum velocity or maximum stall force. Also, the potential strength used in the model was relatively small and, in an experiment, electro-osmotic effects may well be stronger than electrophoretic forces on the polymer [34], possibly making the potential actually experienced by the polymer more effective. Hence, even though a fully realistic model should include a worm-like chain model, electrostatic screening effects, Coulomb interactions, and hydrodynamic interactions including electro-osmotic flow, we conclude from our simulation results that an experiment appears feasible.

Below we confirm whether our basic conclusions, obtained using a 1D potential, hold also for a more realistic 2D potential qualitatively similar to that created by an interdigitated electrode array.

B. Two-dimensional potential

As a 2D model for the potential created by an experimental device, we consider a periodic array of pairs of oppositely charged, infinitely thin electrodes perpendicular to the x axis in the plane $z=0$. The electrodes in a pair are separated by αL and the periodic spacing between pairs is L. They are alternately charged during t_{on} and uncharged during t_{off}. Two surfaces are introduced into the system to place bounds on

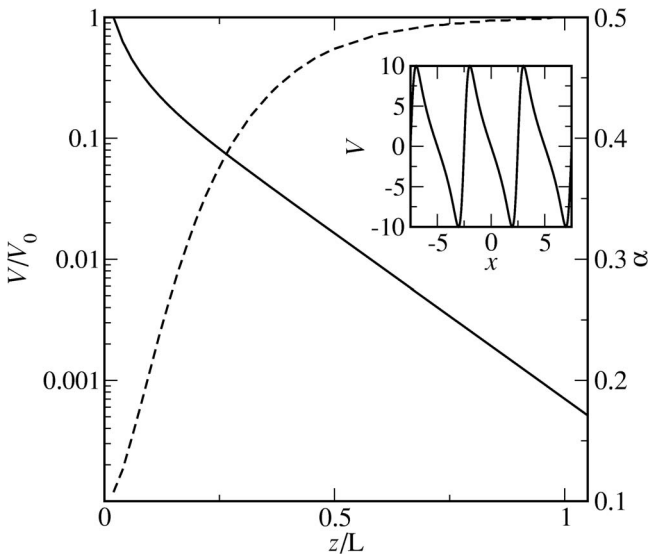

FIG. 15. Characteristics of the potential formed by an electrode array. Solid line; left axis: Decrease in the potential strength with distance from the surface; V_0 is an arbitrary scaling factor. Dashed line; right axis: Effective asymmetry measured by the separation of the maxima and minima of the potential as a fraction of L. Inset: The x dependence of the potential at a distance 0.5σ from the surface ($L=5\sigma$).

the diffusion of the polymer along the z axis. These are of the same form as Eq. (1), with the monomer-surface distance replacing the interparticle separation. The surfaces are placed at the positions $z_1=-0.5\sigma$ and $z_2=100\sigma$. If the upper surface, z_2, corresponds to a cover slip, then the experimental system would consist of a micro-chamber with a realistic height of approximately 10 μm.

Screening effects due to solvent counter-ions are ignored. As shown in Fig. 15(a), both the absolute value and the effective asymmetry of the electrostatic potential produced by the electrode array fall off within a distance L from the surface. Because of the short-range nature of the potential, it is necessary to use stronger fields than previously in order to achieve processive motion. The potential is scaled such that the difference between maxima and minima is $20kT$ for $z=0.5\sigma$.

The polymer velocity as a function of L has similar behavior to the simpler potential, exhibiting a peak at $L \approx 5\sigma$ for $t_{off}=20\tau$ and at $L \approx 7\sigma$ for $t_{off}=40\tau$ [Fig. 16(a)]. The average velocities achieved in the 1D and 2D cases are of the same order of magnitude.

In Fig. 16(b), the trace of the polymer position with time is shown for $L=5\sigma$ and $t_{off}=20\tau$. Regions can be seen where the polymer diffuses beyond the attractive region of the potential in the z direction and undergoes a free random walk. The duration of this random walk is characterized by an average return time, which depends on the position of the wall at z_2. If the polymer is confined to a smaller space by reducing the separation z_2-z_1, the return time will be lower and the velocity as measured by the total displacement in x over a given fixed time will be higher. The ability of the polymer to "detach" from the surface is strongly dependent on the ratchet period and, consequently, ratcheting is poor for

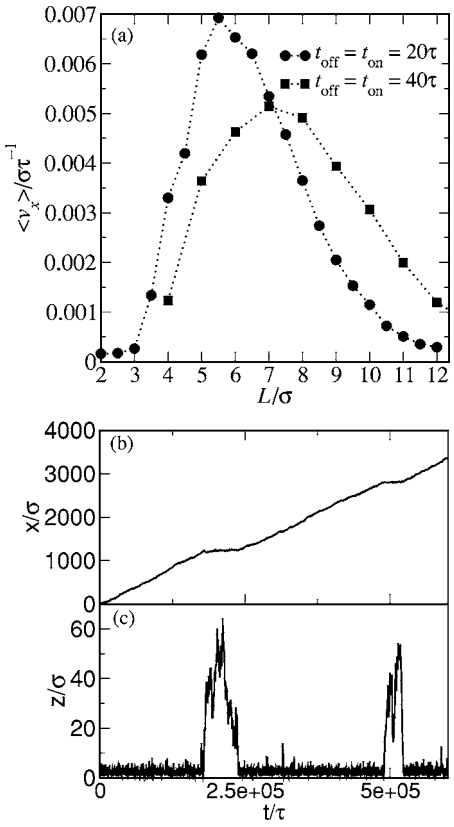

FIG. 16. (a) Velocity of a polymer in a ratchet formed by an array of electrodes as a function of ratchet spatial period. (b) Trace of the polymer position along the x axis (top) and z axis (bottom) for $L=5\sigma$ ($N=50$; $t_{on}=t_{off}=20\tau$).

shorter periods, as shown by the rapid drop in velocity for short values of L in Fig. 16(a).

V. CONCLUSIONS

We have performed Brownian dynamics simulations of a single molecule motor based on a polymer in a flashing ratchet. In contrast to single particles in a flashing ratchet, the polymer motor does not rely on center-of-mass diffusion, but on thermally activated conformational changes. This central role of the molecule's internal degrees of freedom is reflected in key aspects of motor performance: First, the motor velocity decreases with polymer size much more slowly than for single particles in a flashing ratchet. Second, whereas for single particles in a ratchet the stall force *decreases* with particle size, the stall force for the polymer motor *increases* with N. The physical reason is that only part of the polymer needs to diffuse against an external force to induce stepping of the entire polymer during t_{on}, which effectively constitutes a power stroke. On a fundamental level, this feature is akin to dimeric biomolecular motors, which also make use of internal degrees of freedom to increase their stall force beyond that possible for a monomeric motor. In contrast to biomolecular motors, however, we find that the very large number of degrees of freedom in our polymer leads to a very small motor efficiency. Future work will consider the internal energetics of the polymer and the role that fluctuations and flexibility have on performance and efficiency. It is likely that a finite, but small, number of functionally well-chosen internal degrees of freedom (as selected by biological evolution) yields the best performance. Most importantly, however, it appears that our motor can be realized experimentally. This study, therefore, points the way not only to the real-time study of the performance of an artificial, single-molecule motor, but perhaps also to the first experimental realization of a microscopic, coupled Brownian motor system that draws on cooperative effects to increase performance.

In the present calculations, we have ignored both hydrodynamic interactions and electrostatic screening. While screening can be incorporated quite easily, hydrodynamic interactions present considerably greater difficulties. It is known [36] that the dependence of the diffusion coefficient of a polymer scales as $1/R_g$ rather than as $1/N$ in an explicit solvent and, therefore, we expect that some quantitative differences from our results will be found experimentally. However, we believe that our conclusions are qualitatively robust.

ACKNOWLEDGMENTS

We acknowledge helpful discussions with Brian Long and support by the National Science Foundation (PHY 0239764) to H.L., by NSF-IGERT and by NSF GK-12 (E.C.); M.J.Z. and M.P. wish to thank NSERC of Canada for a Discovery grant. This research has been enabled by the use of West Grid computing resources, which are funded in part by the Canada Foundation for Innovation, Alberta Innovation and Science, BC Advanced Education, and the participating research institutions. West Grid equipment is provided by IBM, Hewlett Packard and SGI. We wish to thank the IRMACS Center at Simon Fraser University for the use of its superb facilities. M.J.Z. also wishes to thank John Bechhoefer, David Boal, Nancy Forde, Kurt Kremer, Fredericke Schmid, Depankar Sen, and Gary Slater for useful discussions and correspondence.

[1] F. Jülicher, A. Ajdari, and J. Prost, Rev. Mod. Phys. **69**, 1269 (1997).
[2] M. Schliwa and G. Woehlke, Nature (London) **422**, 759 (2003).
[3] R. D. Vale and R. A. Milliagan, Science **288**, 88 (2000).
[4] J. Howard, *Mechanics of Motor Proteins and the Cytoskeleton* (Sinauer, Sunderland, MA, 2001).
[5] D. Bray, *Cell Movements—From Molecules to Motility* (Garland, New York, 2001).
[6] B. Alberts, D. Bray, J. Lewis, M. Raff, K. Roberts, and J. D. Watson, *Molecular Biology of the Cell*, 3rd ed. (Garland, New York, 1994).

[7] V. Balzani, A. Credi, F. Raymo, and J. F. Stoddart, Angew. Chem., Int. Ed. **39**, 3348 (2000).
[8] R. T. Kelly, H. de Silva, and R. A. Silva, Nature (London) **401**, 152 (1999).
[9] N. Koumura, R. W. J. Zijstra, R. A. van Delden, N. Harada, and B. L. Feringa, Nature (London) **401**, 152 (1999).
[10] B. Yurke, A. J. Turberfield, A. P. Mills, F. C. Simmel, and J. L. Neumann, Nature (London) **406**, 605 (2000).
[11] F. C. Simmel and B. Yurke, Phys. Rev. E **63**, 041913 (2001).
[12] W. Sherman and N. Seeman, Nano Lett. **4**, 1203 (2004).
[13] P. Yin, H. Yan, X. Daniell, A. Turberfield, and J. Reif, Angew. Chem., Int. Ed. **43**, 4906 (2004).
[14] R. Bartussek and P. Hänggi, Phys. Bl. **51**, 506 (1995).
[15] P. Hänggi, R. Bartussek, P. Talkner, and J. Luczka, Europhys. Lett. **35**, 315 (1996).
[16] R. D. Astumian, Science **276**, 917 (1997).
[17] R. D. Astumian and P. Hänggi, Phys. Today **55**(11), 33 (2002).
[18] P. Reimann, Phys. Rep. **361**, 57 (2002).
[19] H. Linke, Appl. Phys. A: Mater. Sci. Process. **75**, 167 (2002).
[20] A. Ajdari and J. Prost, C. R. Acad. Sci., Ser. II: Mec., Phys., Chim., Sci. Terre Univers **315**, 1635 (1992).
[21] R. D. Astumian and M. Bier, Phys. Rev. Lett. **72**, 1766 (1994).
[22] M. O. Magnasco, Phys. Rev. Lett. **71**, 1477 (1993).
[23] C. R. Doering, W. Horsthemke, and J. Riordan, Phys. Rev. Lett. **72**, 2984 (1994).
[24] T. E. Dialynas and G. P. Tsironis, Phys. Lett. A **218**, 292 (1996).
[25] H. Y. Wang and J. D. Bao, Physica A **337**, 13 (2004).
[26] S. Klumpp, A. Mielke, and C. Wald, Phys. Rev. E **63**, 031914 (2001).
[27] G. N. Stratopoulos, T. E. Dialynas, and G. P. Tsironis, Phys. Lett. A **252**, 151 (1999).
[28] J. S. Bader, R. W. Hammond, S. A. Henck, M. W. Deem, G. A. McDermott, J. M. Bustillo, J. W. Simpson, G. T. Mulhern, and J. M. Rothberg, Proc. Natl. Acad. Sci. U.S.A. **96**, 13165 (1999).
[29] R. W. Hammond, J. S. Bader, S. A. Henck, M. W. Deem, G. A. McDermott, J. M. Bustillo, and J. M. Rothberg, Electrophoresis **21**, 74 (2000).
[30] K. Kremer and G. S. Grest, J. Chem. Phys. **92**, 5057 (1990).
[31] C. Baumann, S. Smith, V. Bloomfield, and C. Bustamante, Proc. Natl. Acad. Sci. U.S.A. **94**, 6185 (1997).
[32] C. Bouchiat, M. D. Wang, J.-F. Allemand, T. Strick, and S. M. Block, Biophys. J. **76**, 409 (1999).
[33] G. W. Slater, Y. Gratton, M. Kenward, L. McCormick, and F. Tessier, Soft Mater. **1**, 365 (2003).
[34] W. D. Volkmuth and R. H. Austin, Nature (London) **358**, 600 (1992).
[35] M.-K. Liu and J. Giddings, Macromolecules **26**, 3576 (1993).
[36] M. Doi and S. F. Edwards, *The Theory of Polymer Dynamics* (Oxford University Press, Oxford, 1986).
[37] H. Linke, M. T. Downton, and M. J. Zuckermann, Chaos **15**, 026111 (2005).
[38] J. A. Freund and L. Schimansky-Geier, Phys. Rev. E **60**, 1304 (1999).
[39] M. E. Fisher and A. B. Kolomeisky, Physica A **274**, 241 (1999).
[40] M. E. Fisher and A. B. Kolomeisky, Proc. Natl. Acad. Sci. U.S.A. **96**, 6597 (1999).
[41] C. M. Coppin, D. W. Pierce, L. Hsu, and R. D. Vale, Proc. Natl. Acad. Sci. U.S.A. **94**, 8539 (1997).
[42] K. Sekimoto, J. Phys. Soc. Jpn. **66**, 1234 (1997).
[43] I. Derényi, M. Bier, and R. D. Astumian, Phys. Rev. Lett. **83**, 903 (1999).
[44] J. M. R. Parrondo and B. J. de Cisneros, Appl. Phys. A: Mater. Sci. Process. **A75**, 179 (2002).
[45] D. Suzuki and T. Munakata, Phys. Rev. E **68**, 021906 (2003).
[46] L. Machura, M. Kostur, P. Talkner, J. Luczka, F. Marchesoni, and P. Hänggi, Phys. Rev. E **70**, 061105 (2004).
[47] J. M. R. Parrondo, J. M. Blanco, F. J. Cao, and R. Brito, Europhys. Lett. **43**, 248 (1998).
[48] J. S. Bader, M. W. Deem, R. W. Hammond, S. A. Henck, J. W. Simpson, and J. M. Rothberg, Appl. Phys. A: Mater. Sci. Process. **75**, 275 (2002).
[49] A simple scaling argument based on the assumptions of Ajdari and Prost [20] gives the L dependence of the average velocity as $v(L;D_2)=\sqrt{D_2/D_1}v(\sqrt{D_2/D_1}L;D_1)$. For the range of polymer diffusion constants that we have investigated here we would expect that the maximum velocity would decrease by a factor of approximately 4.5 for a single particle with no internal degrees of freedom and that the position of the peak would also scale by a similar amount.
[50] Supporting animations are available at http://www.sfu.ca/~mdownton/pre_supporting/
[51] This regime is not shown in Fig. 11 because here we keep the potential height V (see Fig. 1) constant when we increase L, reducing the force the ratchet exerts on the polymer. This method is unsuitable for large L.